A model study of the growth of summer monsoon disturbances

S. V. Kasture, R. N. Keshavamurty* and V. Satyan

Physical Research Laboratory, Ahmedabad 380 009, India
*Indian Institute of Tropical Meteorology, Pune 411 008, India

Using an appropriate north-south distribution of a diabatic heating in a global multilevel spectral model, we have generated summer monsoon type of basic flow. Then we superimposed a pulse at the point of inflexion to the north of the jet at 900 mb. Using conditional instability of the second kind (CISK) type of cumulus heating we integrated the model keeping the basic flow fixed. We found that the pulse grows into observed type of monsoon depression. When cumulus heating was absent the pulse did not show any appreciable growth. The detailed computations of energetics show that the main growth mechanism of the pulse is by baroclinic energy exchange in the presence of cumulus heating.

MONSOON disturbances which form over north Bay of Bengal and move westnorth-westwards across central and adjoining north India are the main rain-producing systems during the summer monsoon season. There have been many studies about the mechanisms of formation and the structure of these disturbances. The studies for understanding the mechanisms of formation fall into mainly two categories: (i) Instability studies of the monsoon flow with horizontal and vertical shears[1-4] and with the inclusion of cumulus heating[5-13], (ii) Numerical model studies[14,15] where the growth of monsoon depressions is predicted from the observed data and calculations of energy conversion are done. The consensus of most of these studies is that monsoon disturbances grow as a result of combined barotropic–baroclinic instability of monsoon flow in the presence of cumulus heating. There have also been calculations showing that cumulus heating destabilizes baroclinic modes[12]. In numerical models calculations of energy conversions yield large values for A_E to K_E (eddy available potential energy to eddy kinetic energy) in the presence of cumulus heating. Conversion of K_Z to K_E (zonal kinetic energy to eddy kinetic energy) is small contrary to suggestions of some linear studies.

We feel that there is a strong need for a third kind of studies where the nonlinear evolution of monsoon perturbations is studied using idealized basic flows with cumulus heating and for doing detailed calculations of energetics. Such studies can clarify many of the dichotomies which exist between linear studies and nonlinear numerical model studies with real data.

In the present study we generated a monsoon zonal flow which has both meridional and vertical shear by imposing an appropriate heating distribution in a global spectral model. Then a weak pulse perturbation was superposed on the basic flow at the point of inflexion and cumulus heating was switched on. The nonlinear evolution of the growing perturbation was studied.

Model study

We have used an atmospheric model based on the primitive equations. It is a global spectral model (in σ coordinates) with five levels in the vertical and rhomboidal truncation at 35 waves corresponding to a horizontal resolution of 2° latitude by 2.8° longitude. The model formulation has been described in Keshavamurty *et al.*[16]. It has ∇^2 type diffusion and linear drag of five days. It has no topography. In the model, an appropriate south to north zonally symmetric diabatic heating distribution $\dot{Q}(y,\sigma)$ is imposed. The model is then run up to 25 days till a steady state is reached. The heating profile $\dot{Q}(y,\sigma)$ is adjusted such that fairly realistic zonal winds are generated. The idealized basic monsoon flow thus generated is shown in Figure 1 (*a*, *b*), with U profiles at 900 mb (maximum westerly of 10 msec^{-1}) and 100 mb (maximum easterly 27 msec^{-1}). Figure 2 shows the meridional profile of gradient of potential vorticity (quasi-geostrophic) at 900 mb of the generated basic flow. It is seen that this changes sign near 21° N. This indicates the possibility of combined barotropic–baroclinic instability.

Next a small pulse perturbation (ψ) is superposed at 900 mb (21° N, 90° E) (Figure 3*a*). It is a pulse with a half width of 4° in latitude and 5.6° in longitude having magnitude of zonal wind 0.5 mps (Figure 3*b*).

$$\psi(x,y) = A\, e^{-c\left(\frac{x-x_1}{a}\right)^2} e^{-c\left(\frac{y-y_1}{b}\right)^2}, \qquad (1)$$

where $a=1.7$, $b=2.4$, $c=0.5$, $y_1=21$ N, $x_1=90$ E, $A=2.25\times10^{-8}$.

The amplitude of the pulse falls to half its central value at the nearest neighbouring grid points. It is superposed at the inflexion point in the low level basic

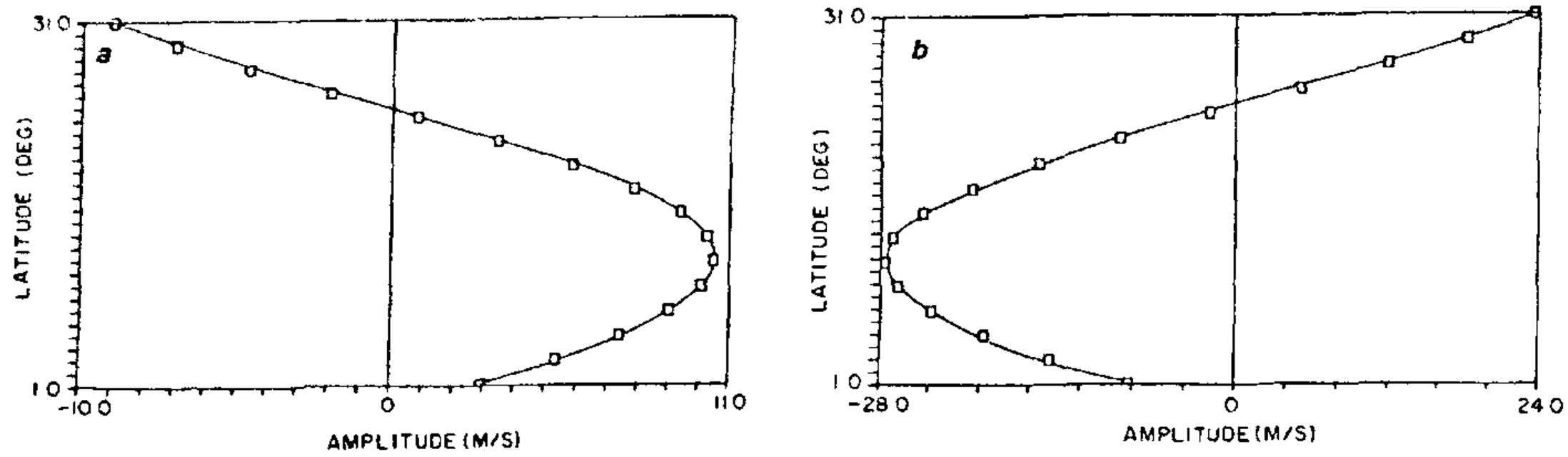

Figure 1. Model simulated zonal wind (U) profile at 900 mb (*a*) and 100 mb (*b*) in m/s.

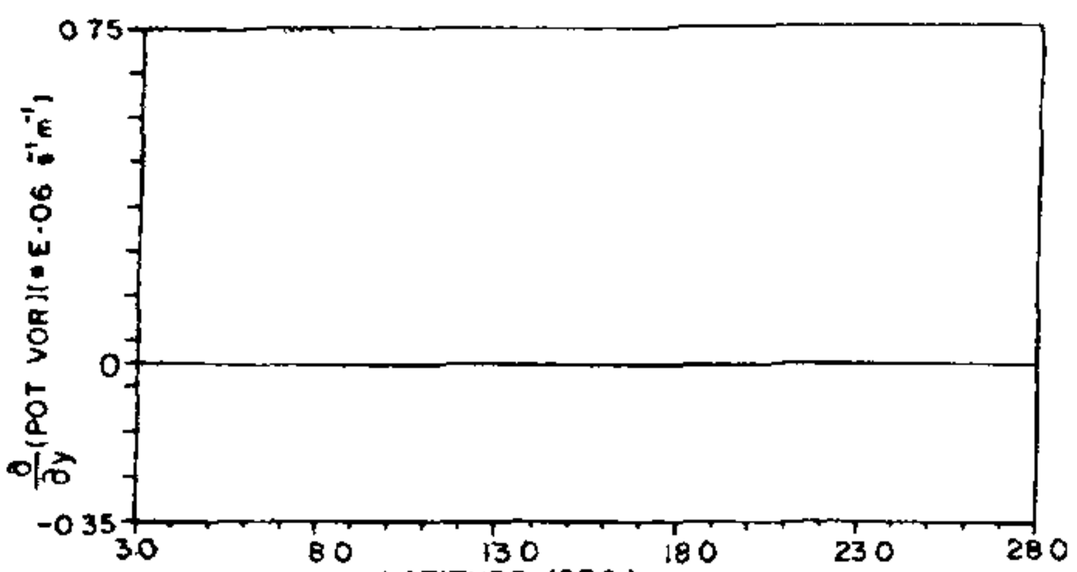

Figure 2. Meridional profile of gradient of potential vorticity of the basic flow at 900 mb ($m^{-1}s^{-1}$).

flow at 21° N latitude, i.e. to the north of the low level jet. Next cumulus heating $\dot{Q}$ is switched on. For $\dot{Q}$ we have used the simplified cumulus conditional instability of the second kind (CSIK) heating scheme of Charney and Eliassen[17],

where

$$\frac{\dot{Q}}{C_p} = H_f(p)\frac{p}{R}s\left[\rho g\sqrt{\frac{K_e}{2f_0}}\sin(2\alpha_s)\zeta_{900}\right] \times 0.5 \times \pi \times \sin(\pi\sigma_L).$$

where $H_f(p) = 1.5$, and the various symbols have the following meanings: R is the gas constant, s the static stability, ρ the density of air, K_e the eddy viscosity coefficient, α_s the surface cross-isobaric angle, and ζ_{900} represents vorticity at 900 mb due to pulse.

The vertical profile of the cumulus heating used here is based on the study of Mohanty and Das[18]. It has a maximum of cumulus heating at 500 mb. Therefore a vertical distribution of the form sin ($\pi\sigma$) was used. The model equations are integrated for five days keeping the basic flow fixed, to study the time evolution of the pulse.

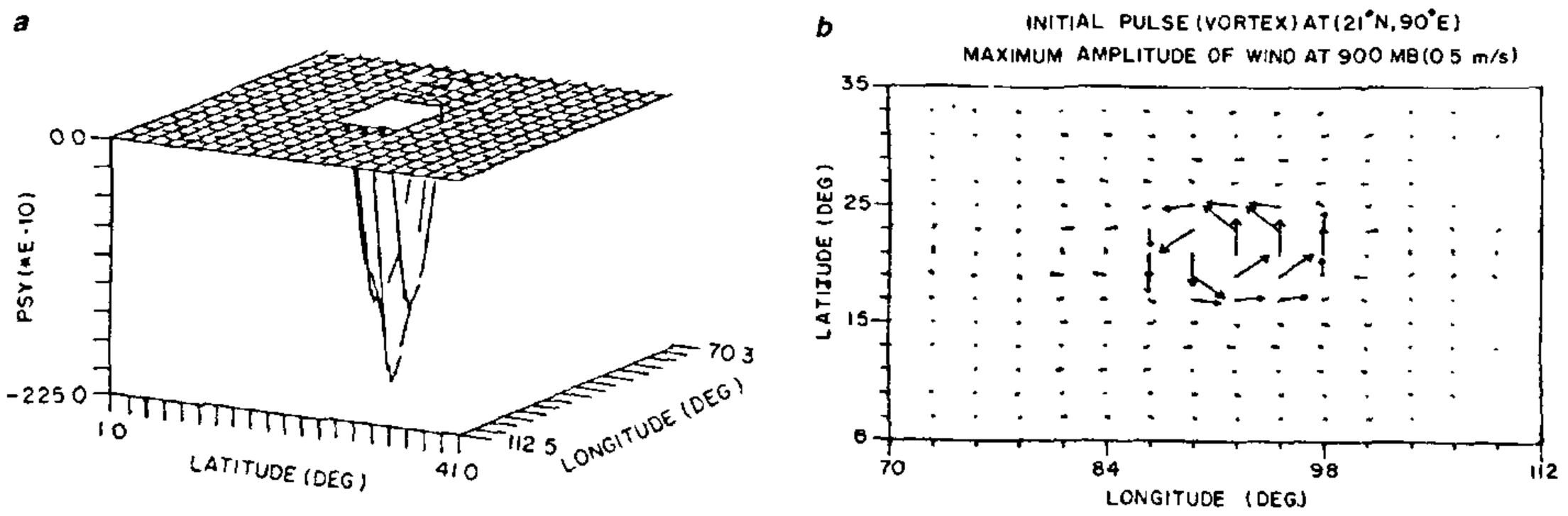

Figure 3. Pulse in ψ ($m^2 s^{-1}$) (three-dimensional view) at 900 mb (21° N, 90 E) (*a*), pulse (vortex) at 900 mb having maximum amplitude of wind 0 5 ms^{-1} (*b*)

Results and discussion

Characteristics of the growing disturbance

Figures 4 *a–e* show the total wind field for the first five days (in the case of the incipient vortex superimposed to the north of the low level jet). It is clearly seen from the figures that cyclonic flow around the centre of the perturbation has steadily grown in strength from day 1 to day 5. The vortex is strongest in the lower troposphere. The maximum amplitude of the perturbation wind increased to 1, 2.1, 4.6, 8.7 and 20 m/s on the first, second, third fourth and fifth day respectively. Figure 5 shows the perturbation wind field on the fifth day. It is clear that the perturbation has grown into depression strength (20 m/s) on the fifth day and its scale is around 2000 km.

Figures 6 *a–d* show the east-west section through the

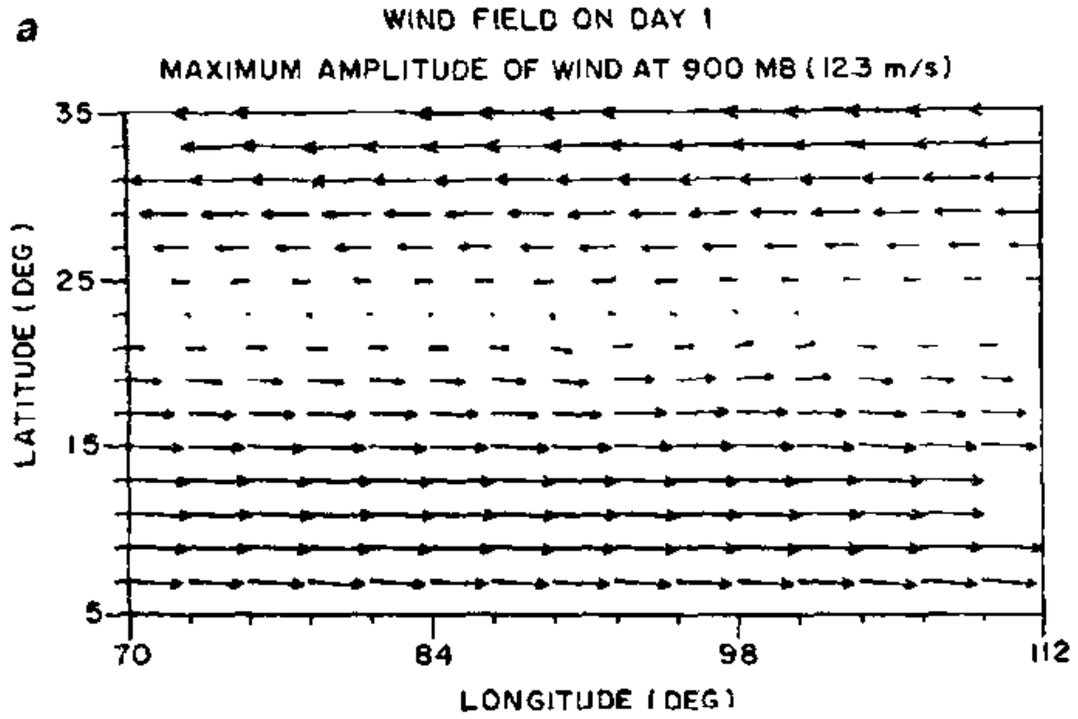

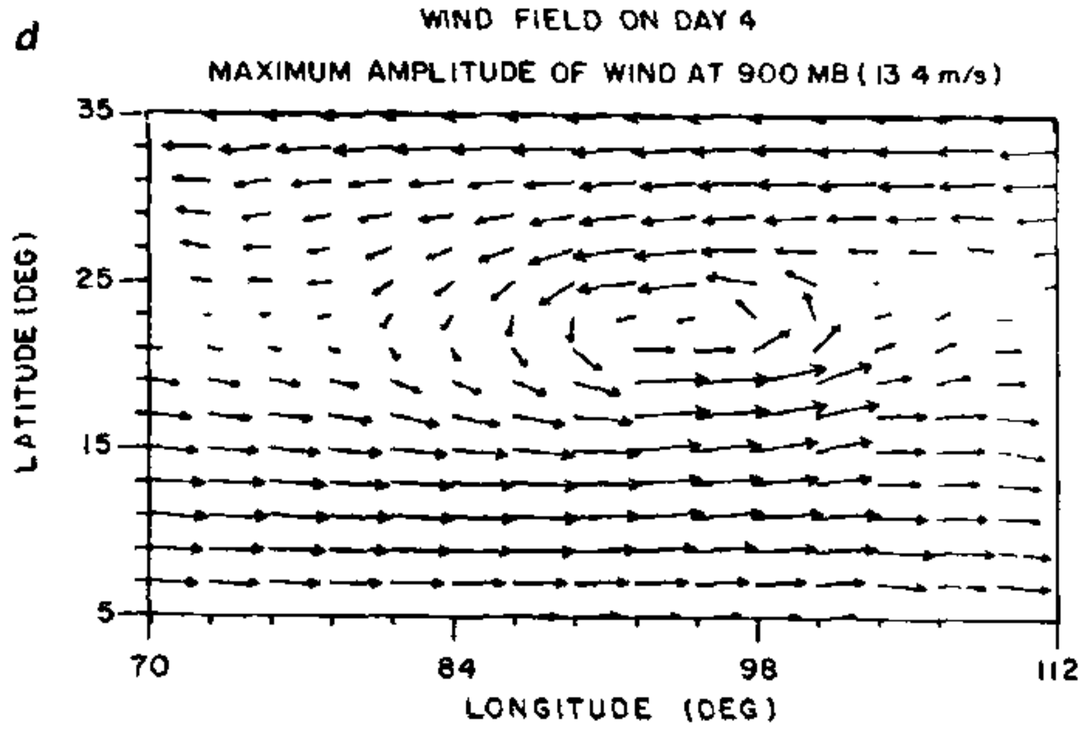

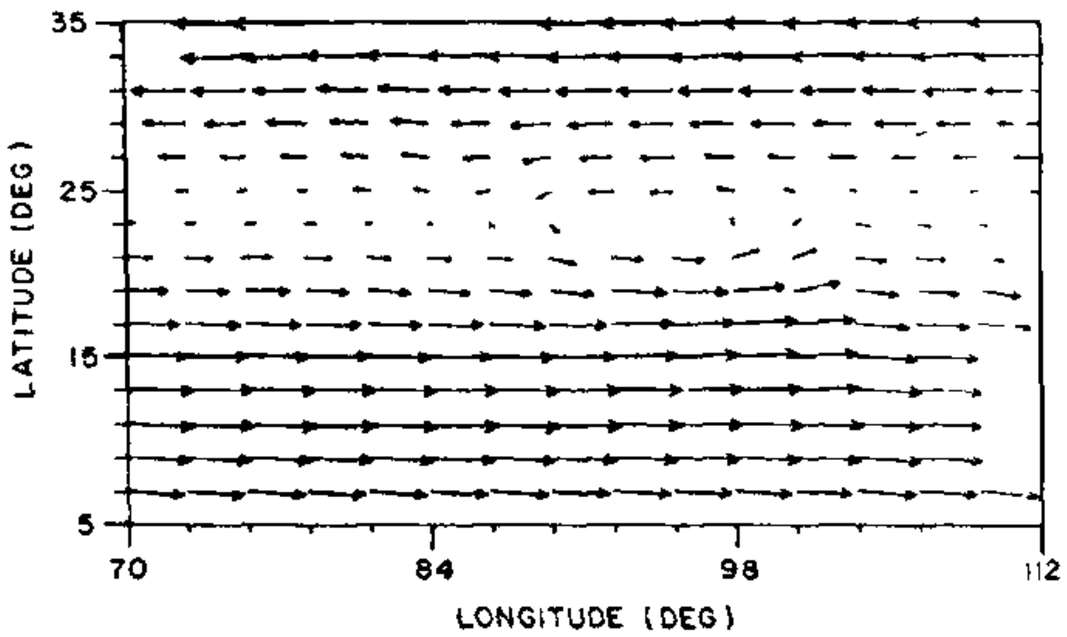

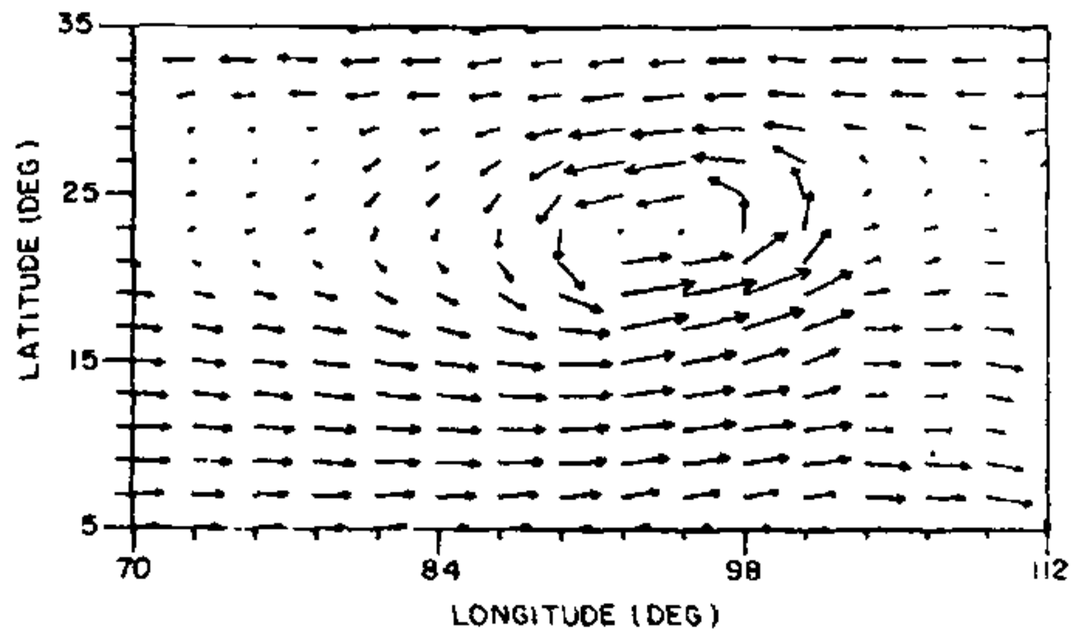

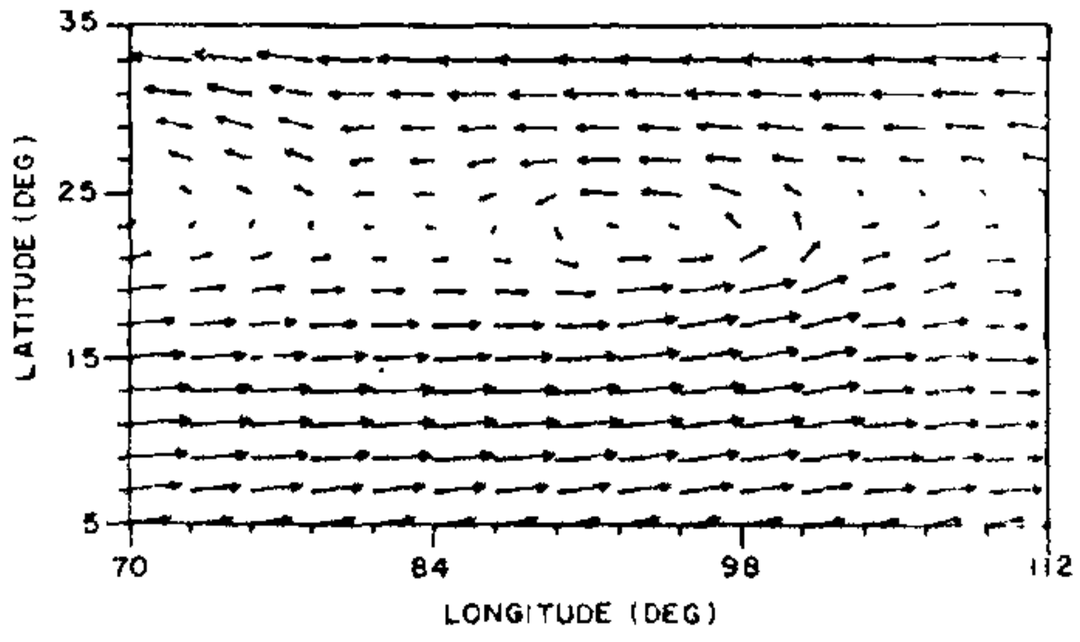

Figure 4. Total wind field at 900 mb on day 1, 2, 3, 4, 5 (*a, b, c, d, e*) having maximum amplitude of wind 12.3, 11.9, 13, 13.4 and 24.5 m/s respectively

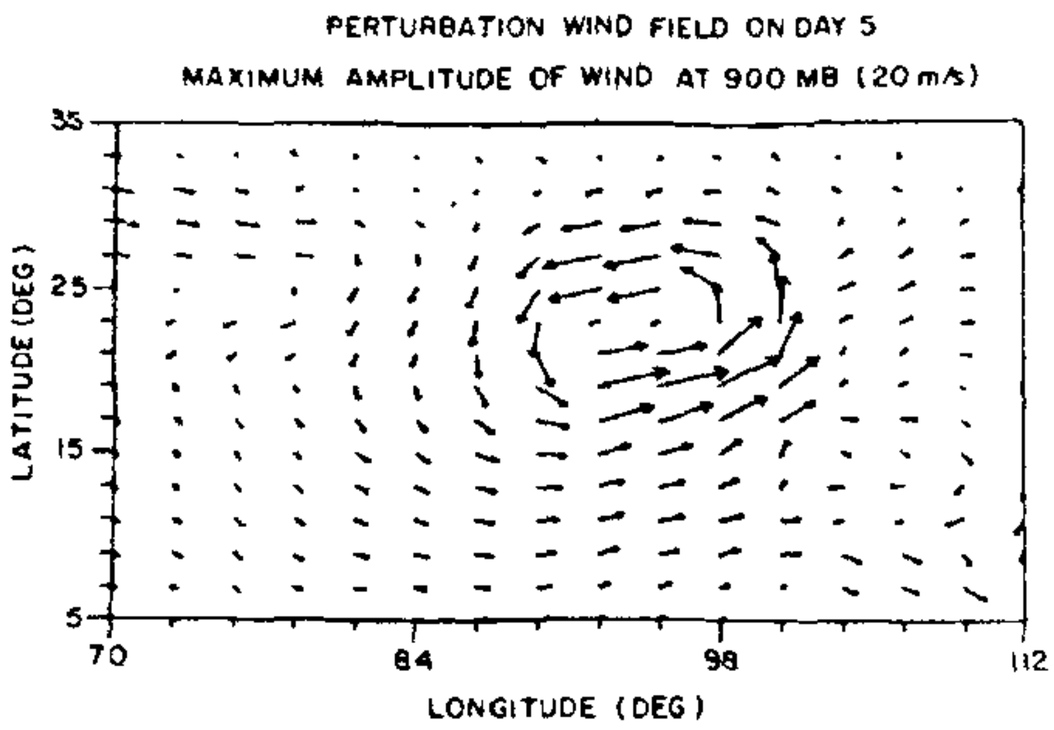

Figure 5. Perturbation wind field at 900 mb on day 5 having maximum amplitude of wind 20 m/s.

centre of the vortex of (i) meridional wind, (ii) vorticity, (iii) divergence, and (iv) temperature on the 4th day. It is seen that the cyclonic circulation extends up to almost 400 mb. Above this there is anticyclonic flow. The warm core extends from 900 mb to 200 mb. Another feature to be noticed is the anticyclonic vorticity on either side of the main vortex, especially to the east of the main cyclonic vortex. All these aspects are in fair agreement with the observed features of monsoon depressions.

A second calculation was done by imposing the pulse at 21°N and the model was integrated for five days without CISK heating. No growth of the pulse was noticed in this case. This shows that only horizontal and vertical shear are not sufficient for the growth of the perturbation but cumulus heating is essential for the growth of the disturbance.

Vertical circulation and energetics

Figures 7 *a–e* show east-west sections of vertical motion through the centre of the depression on the first, second, third, fourth and fifth days. The upward motion at the centre and descending motion on either side is clearly seen. The steady growth of the vertical circulation with time is clearly brought out. A comparison of Figure 6 *d* with 7 *d* brings out that there

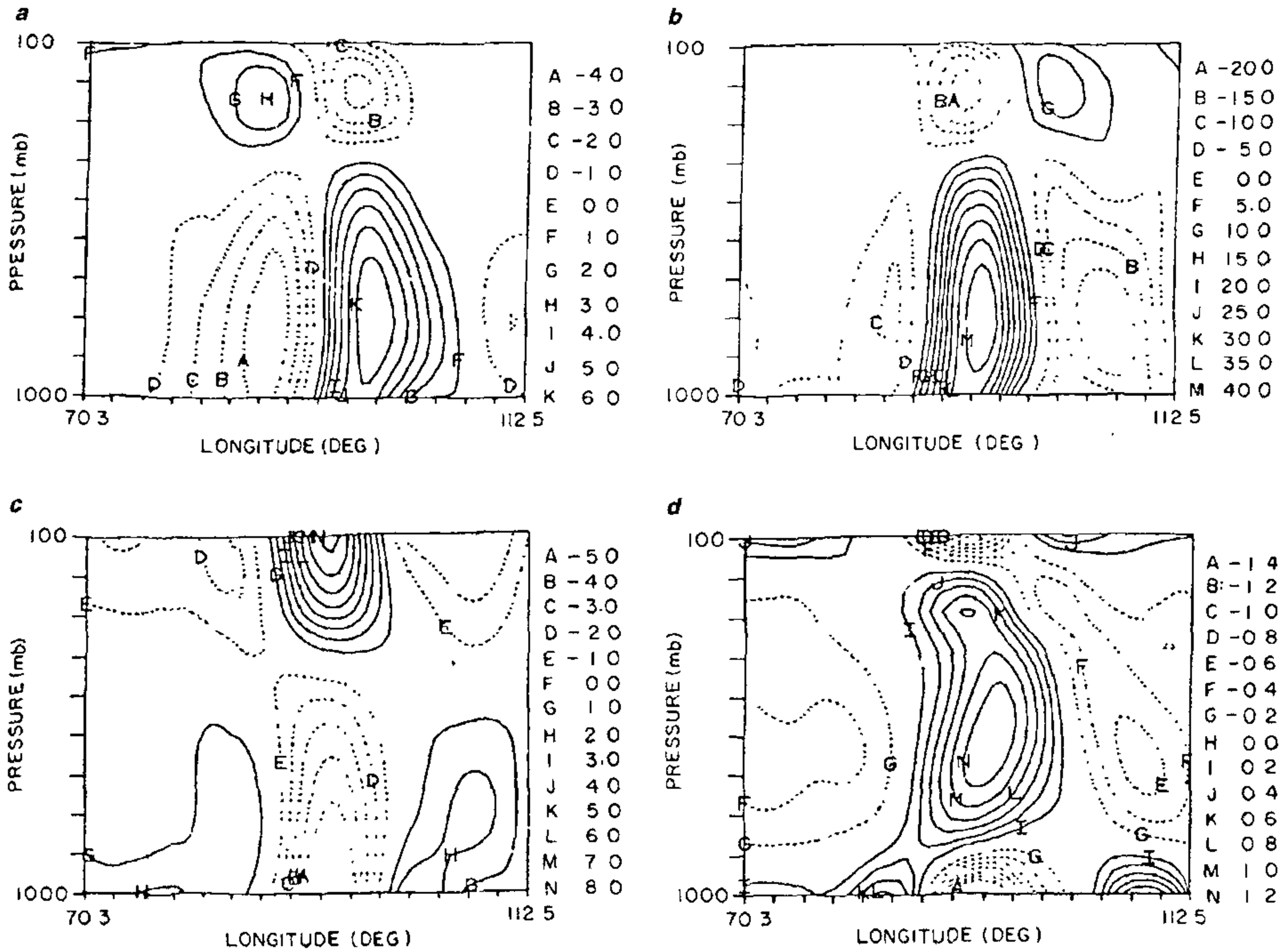

Figure 6. East-west section (*x-p* plot) of meridional wind (*a*), vorticity (*b*), divergence (*c*), temperature (*d*) through the centre of the vortex

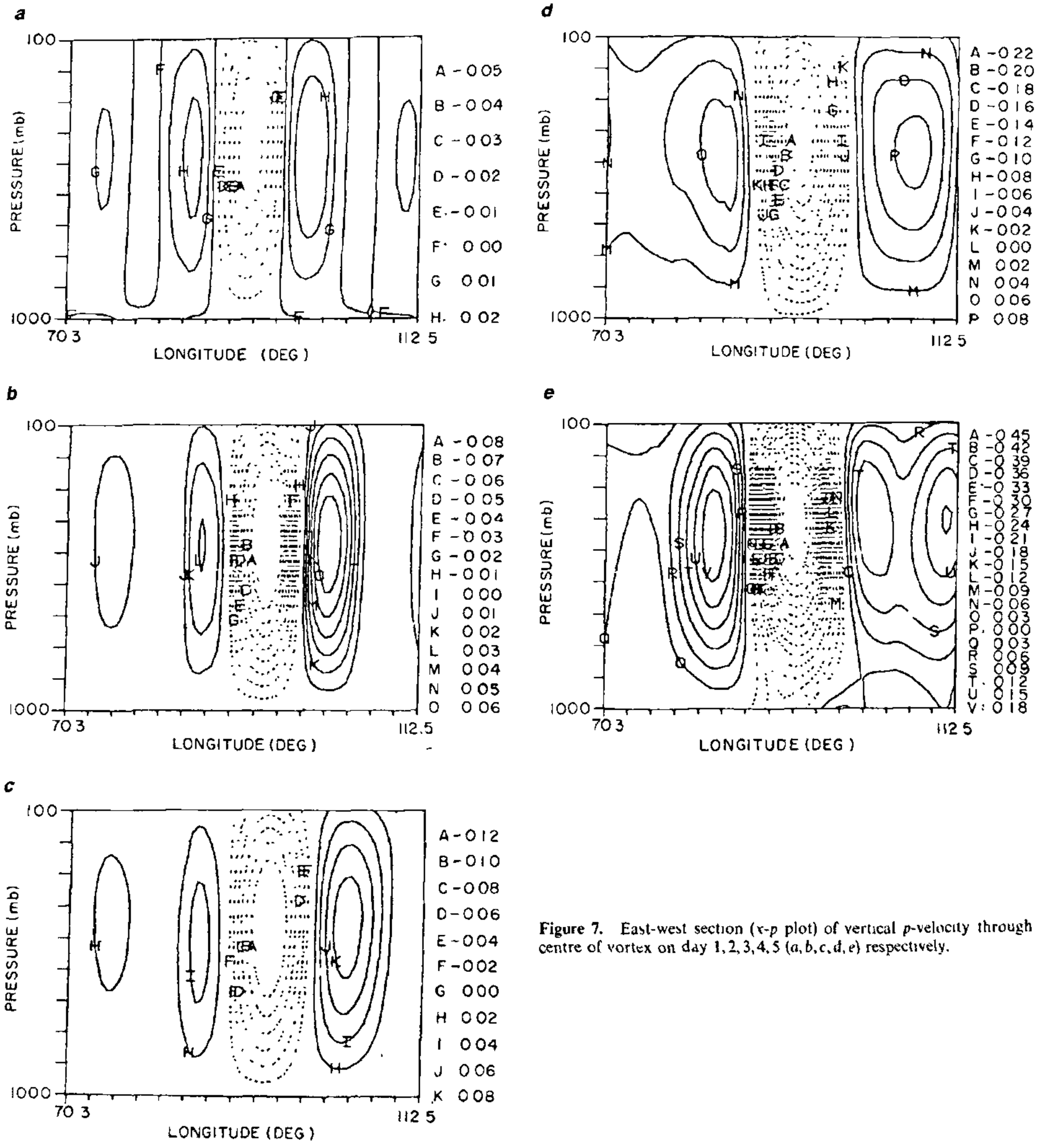

Figure 7. East-west section (x-p plot) of vertical p-velocity through centre of vortex on day 1, 2, 3, 4, 5 (a, b, c, d, e) respectively.

is rising of warm air and sinking of cold air. This results in baroclinic energy conversions and hence growth of the disturbance. In order to see how this simulated depression is maintained we have carried out detailed energetics calculations over the (limited) area surrounding the position of the pulse, i.e. from 1° N to 41° N and 70.3° E to 112.5° E. The expression for different forms of energy can be written as follows (see, for instance Rajamani and Sikdar[19])

$$A_Z = \frac{C_p}{2} \int_M \gamma ([T] - \tilde{T})^2 \, dM, \tag{2}$$

$$A_E = \frac{C_p}{2} \int_M \gamma [T^{*2}] \, dM \tag{3}$$

$$K_Z = \frac{1}{2}\int_M ([u]^2 + [v]^2)\,dM, \tag{4}$$

$$K_E = \frac{1}{2}\int_M ([u^{*2}] + [v^{*2}])\,dM, \tag{5}$$

where A_Z, A_E, K_Z, and K_E are zonal available potential energy, eddy available potential energy, zonal kinetic energy and eddy kinetic energy respectively over closed domain (of mass M) under consideration.

The various energy conversion terms are as follows.

$$C(A_Z, A_E) = -C_p \int_M \gamma \left\{ [v^* T^*] \frac{\partial [T]}{\partial y} + [w^* T^*] \frac{\partial [T]}{\partial p} \right\} dM \tag{6}$$

$$C(A_Z, K_Z) = -R \int_M \frac{1}{p} ([w] - \{w\})([T] - \{T\})\,dM \tag{7}$$

$$C(A_E, K_E) = -R \int_M \frac{1}{p} [w^* T^*]\,dM \tag{8}$$

$$C(K_Z, K_E) = -\int_M \left\{ [u^* v^*] \frac{\partial [u]}{\partial y} + [u^* w^*] \frac{\partial [u]}{\partial p} + [v^* w^*] \frac{\partial [v]}{\partial p} + [v^* v^*] \frac{\partial [v]}{\partial y} \right\} dM, \tag{9}$$

where $\gamma = -\frac{\theta}{T} \frac{R}{C_p P} \left(\frac{\partial \bar{\theta}}{\partial p} \right)^{-1}$

where [ ] = zonal mean, * = deviation from the zonal mean, $\simeq$ = global seasonal mean, { } = average over the limited area.

All other symbols have their usual meaning. Our purpose is to see the various energy transformations of the growing pulse when the basic flow is kept constant and CISK type of convective heating is operative.

It was found that A_Z *and* K_Z were constant with time (figure not shown). This is as expected since the basic flow is kept fixed. Figure 8 shows the plots of A_E and K_E from 1st to 5th day of integration with CISK. K_E increases slowly from day 1 to day 3 and increases rapidly afterwards. A_E also increases slowly up to day 3 but increases more later on.

Figure 9 shows the conversion of A_Z to A_E, A_E to K_E and K_Z to K_E with time. $C(A_Z, A_E)$ and $C(A_E, K_E)$ values are large and are of comparable magnitude. Thus there is large baroclinic energy conversion in the presence of cumulus heating. $C(A_E, K_E)$ is associated with rising of warm air and sinking of cold air (in the east-west plane) which is clearly seen from Figures 6*d* and 7*d*. From Figure 9 it is seen that the barotropic energy conversion from K_Z to K_E is rather small.

Thus from our energy calculations it is clear that the perturbation grows into depression stage by baroclinic energy exchange in presence of cumulus heating. Barotropic energy exchange is rather small.

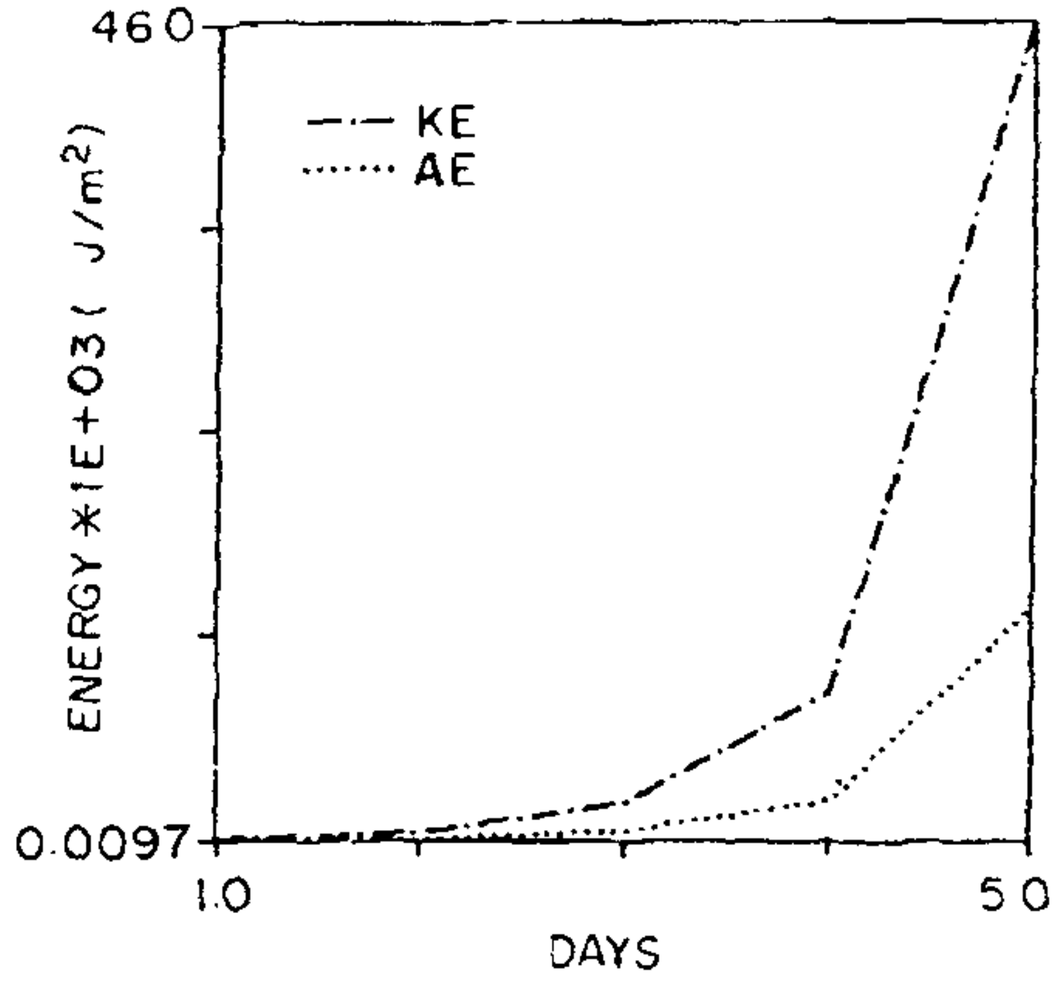

Figure 8. Time variation of vertically integrated eddy available potential energy (A_E) and eddy kinetic energy (K_E) (J m^{-2}).

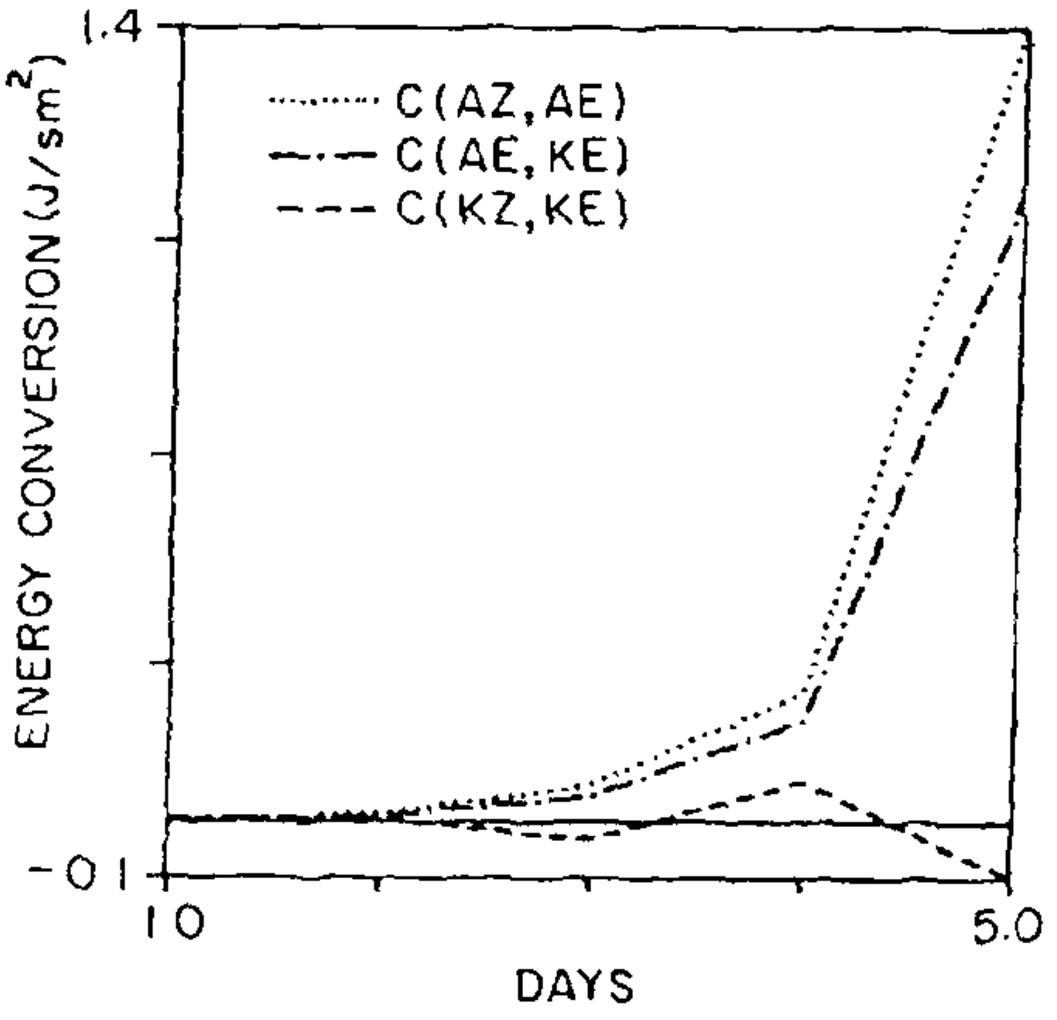

Figure 9. The time variation of vertically integrated energy conversion $C(A_Z, A_E)$, $C(A_E, K_E)$ and $C(K_Z, K_E)$ (Js^{-1} m^{-2})

Conclusions

Our study using summer monsoon type basic flow generated in a global spectral model shows that

- when an incipient vortex is superposed on the low level monsoon type flow in the region of the monsoon trough and cumulus heating is present the vortex grows to depression stage (and further strengthens). The evolving disturbance has many features similar to those of observed monsoon depressions.
- the main growth mechanism is by large-scale baroclinic energy conversions in the presence of cumulus heating.

1. Shukla, J., *Pure Appl. Geophys.*, 1977, **115**, 1449–1461.
2. Keshavamurty, R. N., Asnani, G. C., Pillai, P. V. and Das, S K., *Proc. Indian Acad Sci. (Earth and Planet. Sci.)*, 1978, **A87**, 61–75.
3. Mishra, S K. and Salvekar, P. S., *J. Atmos. Sci.*, 1980, **37**, 383–394.
4. Lindzen, R. S., Farrel, B. and Rossenthal, A. J., *J. Atmos. Sci.*, 1983, **40**, 1178.
5. Shukla, J., *J. Atmos. Sci*, 1978, **35**, 495–508
6. Keshavamurty R. N., Satyan, V. and Goswami, B. N., *Nature*, 1978, **294**, 576.
7. Satyan, V., Keshavamurty, R N, Goswami, B. N, Dash, S. K. and Sinha, H. S. S, *Proc. Indian Acad Sci. (Earth and Planet Sci.)*, 1980, **89**, 277–292.
8. Satyan, V., Keshavamurty, R N. and Goswami, B. N, in *Monsoon Dynamics* (ed Lighthill, J and Pearce, R), Cambridge University Press, London, 1981, pp. 403–413.
9. Goswami, B N., Keshavamurty, R. N. and Satyan, V., *Proc. Indian Acad. Sci (Earth and Planet. Sci.)*, 1980, **89**, 79–97
10. Dash, S. K. and Keshavamurty, R N, *Beitr. Phys. Atmos.*, 1982, **55**, 299–310
11. Mak, M., *J. Atmos Sci.*, 1983a, **40**, 2349–2367.
12. Moorthi, S and Arakawa, A, *J Atmos Sci*, 1985, **42**, 2007–2031.
13. Mak, M, in *Monsoon Meteorology* (ed. Chang, C. P. and Krishnamurti, T. N), Oxford University Press, New York, 1987, pp. 435–460.
14. Krishnamurti, T. N., Pasch, R. J, Pan, H., Chu, S and Ingles, K., *J. Meteor. Soc. Jpn.*, 1983a, **61**, 188–207.
15 Krishnamurti, T. N., Ingles, K, Cocke, S, Kitade, T. and Pasch, R, *J. Meteor. Soc. Jpn*, 1984a, **62**, 613–648.
16. Keshavamurty, R. N, Kasture, S. V. and Krishnakumar, V., *Beitr. Phys Atmos.*, 1986, **59**, 443–454.
17 Charney, J. G. and Eliassen, A., *J. Atmos. Sci.*, 1964, **21**, 68–75.
18 Mohanty, U. C. and Das, S, *Proc. Indian Natl Sci Acad.*, 1986, **52**, 625–640.
19. Rajamani, S. and Sikdar, D. N., *Tellus*, 1989, **A41**, 255–269.

Received 20 August 1992; accepted 5 December 1992

RESEARCH COMMUNICATIONS

Occurrence of ultramafic breccia in the Aravalli Fold Belt, Rajasthan

M. Mohanty, G. P. Gupta and R. L. Sahu
Geological Survey of India, 15–16 Jhalanadungri, Jaipur 302 004, India

A lensoidal body of serpentinite breccia is preserved within the ophiolite melánge of the Aravalli Fold Belt at Modi, Rajasthan. The field, petrographic characters and rock association possibly suggest that the breccia is formed as a consequence of tectonic emplacement of the serpentinite during the closing of the Aravalli basin.

THE Lower Proterozoic Aravalli Fold Belt (AFB) contains ultramafic rocks distributed in two lineaments, viz. the Rakhavdeb in the east and the Kaliguman in the west[1]. The former coincides with the boundary between the continental shelf and deep sea facies rocks of the Aravalli stratigraphy[2] but the latter is restricted to the deep sea sediments. In both the cases the ultramafic and associated rocks occur as a series of composite slivers and possibly represent ophiolite melánges. Though the serpentinized ultramafics form the dominant constituent, the other commonly associated lithologies are banded chert, gabbro, pillowed basalt, carbonates and minor granites. The ultramafics have undergone various degrees of serpentinization and greenschist facies metamorphism. Here we describe a rare occurrence of serpentinite breccia from the western lineament as Modi–Madha ophiolite melánge (MMOM).

The MMOM forms a band of 100 m to 1.5 km wide and extends for more than 50 km from north of Modi to south of Madha (Figure 1) and possibly joins with the ultramafic band at Jharol. The serpentinized ultramafic rocks in it either form a continuous band or occur as lenses of variable dimensions. The contact of these bodies with the Jharol turbidites is always sharp and very often marked by intense mylonitization. The effect of shearing in the serpentinite is rarely preserved but at places a foliation fabric parallel to the contact is well developed. The chert band generally bordering the ultramafic-turbidite contact is intensely sheared and there is a broad parallelism between the mylonite banding and the first foliation (S_1) of the country rock. The chert band along with the serpentinite and carbonates is involved in (map scale) second generation folding, thus suggesting the melange emplacement during the first deformation of the country rock.

The serpentinite breccia occurs as a lensoidal body (100′ × 20′) within the MMOM about 1.5 km east of Modi (24 47′ 15″, 73 ′ 33′ 50″). It is fine grained, light greenish in colour and contain uneven fragments of